ceramics

MDPI

Communication

The Direct Cold Sintering of α-Al_2O_3 Ceramics in a Pure Water Medium

Anastasia A. Kholodkova [1,*], Maxim V. Kornyushin [1], Arseniy N. Khrustalev [2], Levko A. Arbanas [2], Andrey V. Smirnov [2] and Yurii D. Ivakin [3,4]

[1] Statistics Department, Department of Scientific Research Coordination, State University of Management, 109545 Moscow, Russia; maksim.korn0312@yandex.ru
[2] Laboratory of Ceramic Materials and Technology, MIREA—Russian Technological University, 119454 Moscow, Russia; lywn@yandex.ru (A.N.K.); levko.147@icloud.com (L.A.A.); smirnov_av@mirea.ru (A.V.S.)
[3] Mobile Solutions Engineering Center, MIREA—Russian Technological University, 119454 Moscow, Russia; ivakin@kge.msu.ru
[4] Chemistry Department, Lomonosov Moscow State University, 119991 Moscow, Russia
* Correspondence: anastasia.kholodkova@gmail.com

Abstract: Porous α-Al_2O_3 ceramics are a highly sought-after material with a multitude of applications; for example, they are used as filters, substrates, biomedicine materials, etc. Despite the availability of raw materials, a challenge associated with this technology is the high energy budget caused by sintering above 1500 °C. For the cold sintering processing (CSP) of ceramics, lowering the α-Al_2O_3 sintering temperature is one of the most urgent challenges in the background of its rapid development. This paper is the first to demonstrate a solution to this problem using the CSP of α-alumina ceramics in the presence of pure water as a transient liquid. The manufactured materials were examined using XRD analysis; the evolution of their microstructures during CSP was revealed by SEM; and the porosity was evaluated using the Archimedes method. Ceramics with an open porosity up to 36% were produced at 380–450 °C and 220 MPa in 30 min. An increase in the pressure was found to impede α-Al_2O_3 formation from γ-AlOOH. The development of the microstructure was discussed within the framework of the dissolution–precipitation model and homogenous nucleation. The results of the SEM study pointed to the coalescence of γ-AlOOH grains during CSP.

Keywords: gibbsite; boehmite; alumina; cold sintering process; porous ceramics

check for updates

Citation: Kholodkova, A.A.; Kornyushin, M.V.; Khrustalev, A.N.; Arbanas, L.A.; Smirnov, A.V.; Ivakin, Y.D. The Direct Cold Sintering of α-Al_2O_3 Ceramics in a Pure Water Medium. *Ceramics* **2024**, *7*, 1030–1042. https://doi.org/10.3390/ceramics7030067

Academic Editor: Frank Kern

Received: 3 April 2024
Revised: 17 June 2024
Accepted: 1 July 2024
Published: 31 July 2024

Copyright: © 2024 by the authors. Licensee MDPI, Basel, Switzerland. This article is an open access article distributed under the terms and conditions of the Creative Commons Attribution (CC BY) license (https://creativecommons.org/licenses/by/4.0/).

1. Introduction

The cold sintering process (CSP) was first proposed by Randall et al. in their publication in 2016 [1]. Today, CSP is known to be a rapidly developing technique used for the express and energy-saving production of ceramic and composite materials, the range of which is expanding annually. By ensuring the consolidation and sintering of materials at a tremendously lowered temperature, CSP was applied for the manufacturing of ceramics and composites as an alternative to high-temperature and multistage techniques. Most often, the mechanism of cold sintering is explained within the framework of the dissolution–precipitation model [2]. To be more specific, this mechanism has been discussed in other relevant reviews [3–5]. At the initial stage, the transient liquid acts like a temporary technological binder in the uniaxial compaction of powders, facilitating the rearrangement of particles. Next, upon heating, it may partially dissolve the solid particles and transport the substance from high- to low-stress surface regions. At present, more than a hundred compositions of materials, including thermally unstable ones, have been densified via CSP [5–9].

An upgrade in an energy budget embedded in CSP is highly desirable to produce materials with an extremely high sintering temperature, for example, refractories. Several

authors reported success in the manufacturing of electrolyte materials, such as those based on yttria-stabilized zirconia [10–12] and sodium-β-alumina [13], as well as magnesia ceramics [14], via single CSP or combined with a post-heat-treatment (PHT) at a temperature of 1200–1300 °C. Conventionally, these ceramic materials are sintered above 1400 °C. CSP allowed their densification up to 83–93% of the theoretical density, as well as the formation of fine-grained microstructures at temperatures of about 30% of the oxides' melting points. However, such examples remain infrequent against the background of achievements in CSP.

The most stable α-modification of alumina (α-Al_2O_3) is a well-known refractory material (sintered above 1500 °C) with a wide application range, from abrasion to microelectronic and biomedical materials. α-Al_2O_3 is highly appreciated due to the combination of chemical stability, mechanical strength, dielectric properties, biological compatibility, and availability [15–17]. In particular, porous α-Al_2O_3 ceramics are of interest for liquid and gas filters, as well as supports for catalysts and metal–organic frameworks (MOFs) [18–21]. In their review, Ohji et al. [22] classified various approaches used for the preparation of macroporous ceramic structures in four categories: partial sintering, the use of sacrificial templates, the replica technique, and direct foaming. In recent years, alumina porous ceramics were reported to be manufactured by following the methods mentioned above [23–26], as well as via rapidly developing 3D printing techniques [27,28] with the precise control of its pore structure. However, these approaches always exhibit a mixture of the achieved properties on the one hand and multistage energy consumption associated with high-cost auxiliary compounds and equipment on the other.

Several recent works have demonstrated the application of CSP to manufacture alumina ceramics. Herisson de Beauvoir et al. [29] prepared a semi-transparent material consisting of boehmite and amorphous alumina via the processing of aluminum hydroxide hydrate at temperatures up to 400 °C and a pressure of 500 MPa for 30–180 min. PHT at 500 °C in air led to the formation of γ-Al_2O_3. Kang et al. [30] performed the CSP of mixed γ- and α-Al_2O_3 in a medium of glacial acetic acid at 300 °C and 300 MPa for 1 h. PHT above 1250 °C led to highly dense α-Al_2O_3 ceramics. Suleiman et al. [31] applied CSP for the compaction of Al_2O_3-NaCl composites which transformed into porous alumina ceramics on PHT at 1200–1500 °C for 30 min. Later, Gao et al. [32] demonstrated the direct preparation of γ-Al_2O_3 translucent ceramics via CSP in 10 M NaOH at 350 °C and 500 MPa without the need for PHT.

Our previous study [33] showed the capability of CSP combined with spark plasma sintering (SPS) to obtain a porous boehmite material. During the PHT, this material transformed in α-Al_2O_3 ceramics with a porosity of about 60%. In this case, γ-$Al(OH)_3$ was used as a raw powder. Moreover, the formation of α-Al_2O_3 in CSP-SPS conditions was observed at 450 °C and 70 MPa in the presence of 5 wt.% of water, but the material demonstrated a poor transport strength. In the current research, we develop CSP for the direct procurement of porous α-Al_2O_3 ceramics, starting from γ-$Al(OH)_3$ powder, in line with the previous results. This study reveals the effects of the processing temperature and pressure on the phase and microstructural transformations during the CSP of alumina in the presence of pure water.

2. Materials and Methods

Gibbsite γ-$Al(OH)_3$ (>99.6% purity, Pikalevo Alumina Refinery LLC, Pikalevo, Russia) and α-Al_2O_3 (Treibacher Industrie AG, Althofen, Austria) powders were used as starting materials in CSP. The characterization of the initial powders using X-ray diffraction (XRD) and scanning electron microscopy (SEM) is presented in Appendix A (Figures A1 and A2). The mean particle sizes of the γ-$Al(OH)_3$ and α-Al_2O_3 powders were 1.93 and 0.63 μm,. A mixture of 95 wt.% γ-$Al(OH)_3$ and 5 wt.% α-Al_2O_3 was prepared by quintuple joint sieving through a sieve with a 300 μm cell. The role of the α-Al_2O_3 additive was to promote alumina nucleation during the cold sintering. Earlier, such an effect of α-Al_2O_3 seeding was reported for synthesis of its fine crystals in supercritical water [34], as well as for conventional sintering from aluminum hydroxide at a lowered temperature [35].

Following the previous experiments on the CSP of α-Al_2O_3 ceramics [33], the amount of α-Al_2O_3 powder added to gibbsite was 5 wt.%. The prepared mixture (1.000 g) was placed inside a mold, which was equipped with a circular heater and a thermal insulation cover (Figure A3). Then, 0.2 mL of distilled water was poured inside of the mold to obtain a suspension. Graphite sheets separated the inner wall of the mold and the punches from the prepared suspension. The filled mold was placed between the platforms of a uniaxial press. A pressure of 90–350 MPa was applied to it. Then, the mold was heated up to a temperature of 380–450 °C with a rate of 860 °C h^{-1} and held isothermally under the applied pressure for 30 min. After that, the pressure was relieved, and the mold cooled down to room temperature. The obtained ceramic sample was removed from the mold and peeled from graphite sheets.

The phase compositions of the initial powders and obtained ceramic samples were studied by the XRD method using a Rigaku D/Max-2500 diffractometer (Rigaku Corp., Tokyo, Japan). The identification of the phases was provided with the use of the PDF2 database [36]. Diffraction pattern profile fitting was carried out following the Le Bail method by means of the FullProf software (version January 2012) [37]. The initial structural models were taken from the Crystallography Open Database [38]. The Rietveld method [39] was applied for the quantitative phase analysis of ceramic samples. A microstructural study of the powders and ceramics was provided using a Jeol JSM 6380 scanning electron microscope (Jeol Ltd., Tokyo, Japan). Particle and grain size distributions based on measurements in the SEM images were determined using ImageJ software [40]. The density and porosity measurements were carried out following the Archimedes method with the use of kerosene as a saturating liquid.

3. Results

Cold sintering of the gibbsite powder in a mixture with 5 wt.% of α-alumina in the presence of 20 wt.% of distilled water resulted in the formation of solid and transportable ceramic samples (an example is shown in Figure 1).

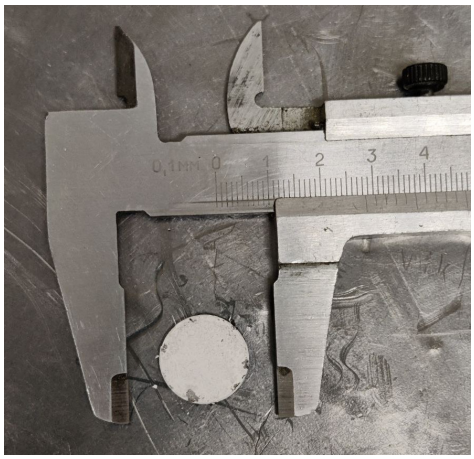
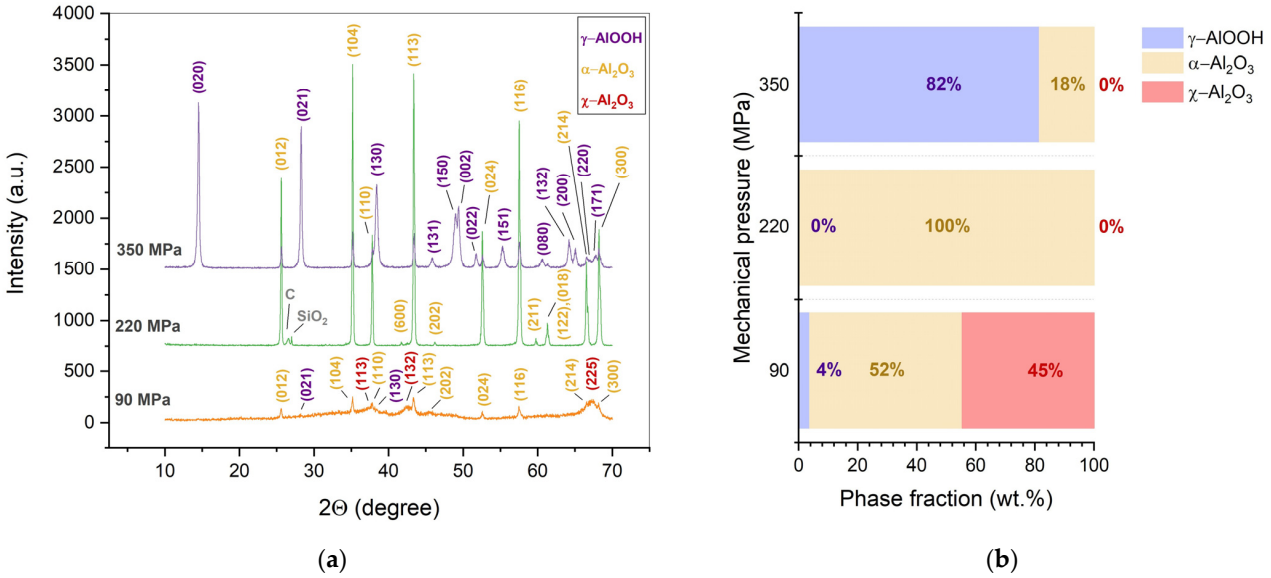


Figure 1. Alumina ceramics manufactured by CSP with an addition of 20 wt.% of distilled water (processing parameters: 450 °C, 220 MPa).

The mechanical pressure initially applied to the mold significantly affected the phase contents of the final ceramic samples. Figure 2a shows the XRD patterns of the samples obtained by CSP at 450 °C under different values of mechanical pressure. At the lowest pressure of 90 MPa, the γ-$Al(OH)_3$ powder transformed into a mixture of α-Al_2O_3 (51.6 wt.%), χ-Al_2O_3, and a small amount of boehmite (γ-AlOOH) (Figure 2b). An increase in pressure up to 220 MPa resulted in the complete transformation of γ-$Al(OH)_3$ into α-alumina. However, further rise of the mechanical pressure to 350 MPa led to the formation of ceramics which consisted of 81.6 wt.% γ-AlOOH and only 18.4 wt.% of α-Al_2O_3 (Figure 2b). The carbon impurity in the XRD pattern originated from the graphite paper, which was in

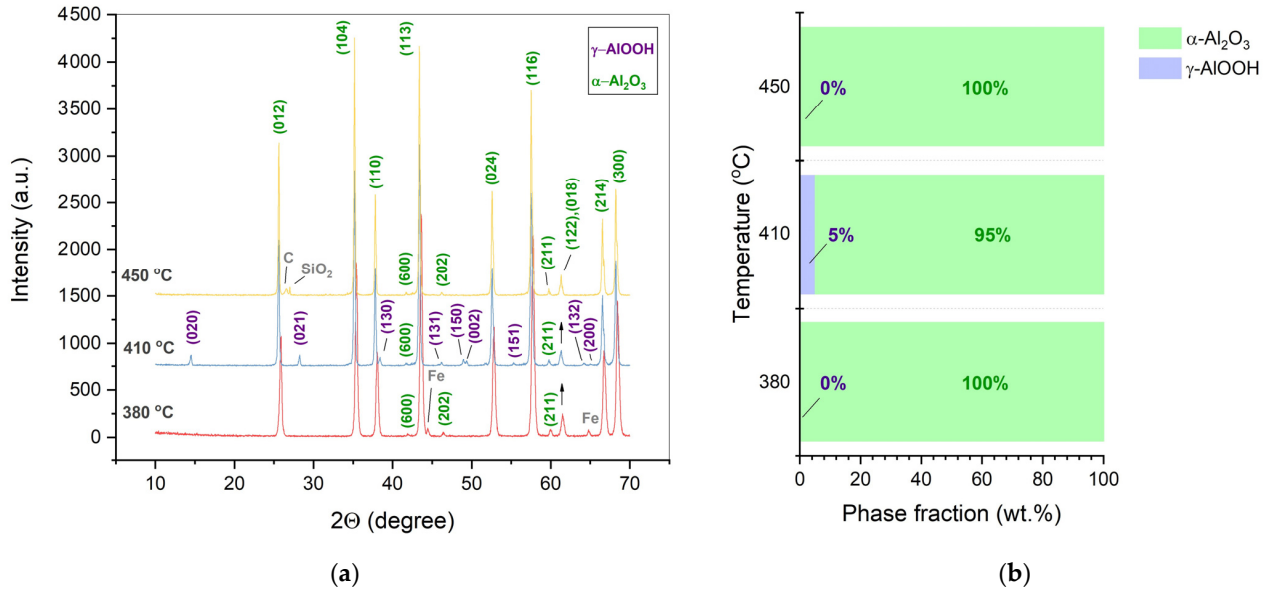
contact with the sample during CSP. The silica impurity came from the mortar used for the ceramics' grinding before the XRD analysis.



(**a**) (**b**)

Figure 2. XRD patterns (**a**) and phase fractions (**b**) of the ceramic samples manufactured by CSP at 450 °C and the indicated mechanical pressure (90–350 MPa). Miller indices correspond to the following phases: γ-AlOOH (PDF2 #000-83-2384), α-Al_2O_3 (PDF2 #000-71-1683), and χ-Al_2O_3 (PDF2 #000-04-0880). Phase fractions are presented excluding foreign impurities.

Figure 3 shows the effect of the CSP temperature on the phase contents of the alumina ceramics at a constant mechanical pressure. A major phase of α-Al_2O_3 was found in the samples obtained at 380–450 °C and a pressure of 220 MPa. However, the ceramics manufactured at 410 °C contained a minor phase of boehmite (γ-AlOOH) in an amount of 5.1 wt.%. This pointed to an incomplete dehydroxylation of the raw material. A metal (Fe) admixture is supposed to be brought into the sample from the inner surfaces of the mold.



(**a**) (**b**)

Figure 3. XRD patterns (**a**) and phase fractions (**b**) of the ceramic samples manufactured by CSP at a pressure of 220 MPa and indicated temperature (380–450 °C). Miller indices correspond to the following phases: γ-AlOOH (PDF2 #000-83-2384) and α-Al_2O_3 (PDF2 #000-71-1683). Phase fractions are presented excluding foreign impurities.

At a mechanical pressure of 350 MPa, the samples formed in a temperature range of 380–450 °C contain a major part of boehmite (Figure 4a). The rise in the CSP temperature resulted in an increase in the α-Al_2O_3 fraction in these samples from 4.9 to 18.4 wt.% (Figure 4b).

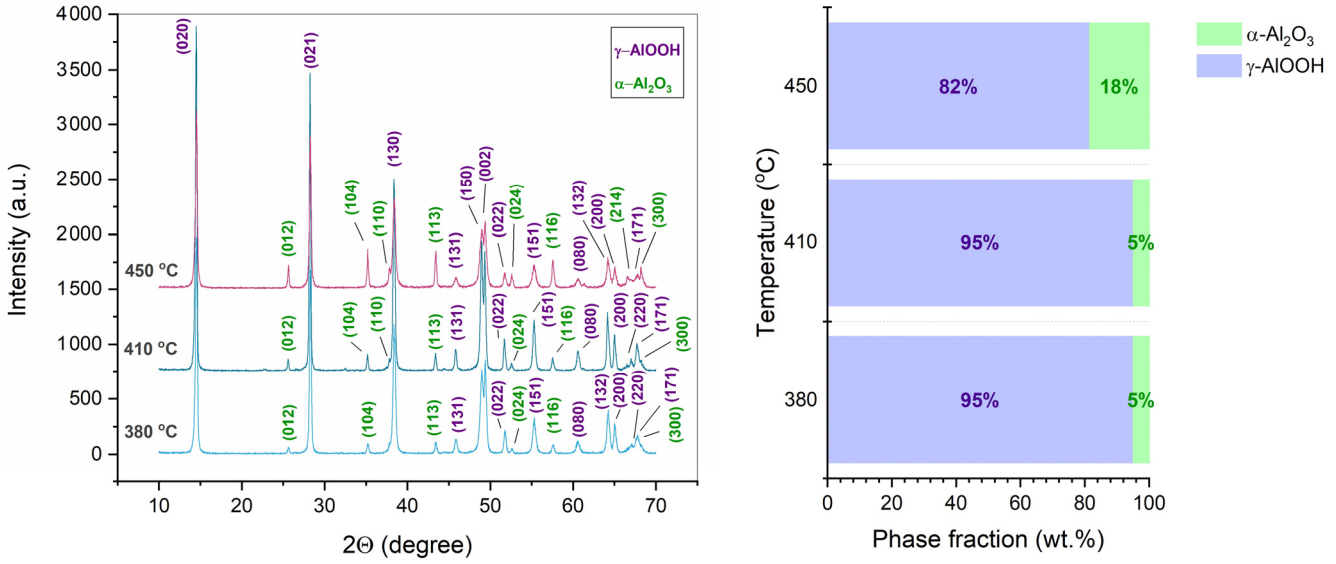


Figure 4. XRD patterns (**a**) and phase fractions (**b**) of the ceramic samples manufactured by CSP at a pressure of 350 MPa and the indicated temperature (380–450 °C). Miller indices correspond to the following phases: γ-AlOOH (PDF2 #000-83-2384) and α-Al_2O_3 (PDF2 #000-71-1683).

The crystallinity of the boehmite and α-Al_2O_3 phases formed in CSP conditions was estimated by their mean crystallite sizes (Table 1). After CSP at 220 MPa, boehmite shows a slightly higher mean crystallite size (6.48 nm) than at 350 MPa (4.94 nm) at an equal temperature of 410 °C. γ-AlOOH to α-Al_2O_3 transformation was accompanied by a decrease in the crystallite size during CSP at 220 MPa. On the opposite, when sintered at a pressure of 350 MPa, α-Al_2O_3 demonstrated an increase in its crystallite size compared to the neighboring boehmite phase. Mostly, the crystallite sizes observed in α-Al_2O_3 were higher in the case of CSP at 350 MPa than at 220 MPa. Low peak intensities in the XRD pattern of the sample obtained at 90 MPa impeded an accurate estimation of crystallite sizes. Under the pressure of 350 MPa, crystallites in both the γ-AlOOH and α-Al_2O_3 phases increased and then decreased with increasing temperature from 380 to 450 °C. In the range of 380–410 °C, the amount of α-Al_2O_3 in prepared ceramics remained close to that initially added to the gibbsite powder. From Figure 4, the proportion of alumina rose to 18 wt.% after the CSP at 450 °C. The newly formed small α-Al_2O_3 crystallites lowered their total average size. An accelerated decomposition similarly affected the mean crystallite size in γ-AlOOH.

The calculated density of the manufactured alumina ceramics was below 65% (Table 1). Open porosity prevailed in the samples obtained at 90 and 220 MPa as well as in ceramics sintered at 380 °C at a pressure of 350 MPa. The lowering of the open porosity in a couple of samples processed at 410 and 450 °C and an applied pressure of 350 MPa indicates the pores' closure in these conditions. The proportion of the closed pores reached 8.0 and 12.8% in the mentioned samples.

A large intergranular pore space was observed in α-Al_2O_3 ceramics obtained at a pressure of 220 MPa and temperatures of 380 and 450 °C (Figure 5). The grains possess mostly irregular shapes and broad size distributions from a submicron size up to tens of microns. The mean values of the grain size of about 3 μm are rather close in these ceramic

samples. Locally, the grains demonstrate intergrowth and coalescence, but their major part is at the stage of neck formation between the neighboring ones.

Table 1. Structural characteristics of the ceramic samples manufactured via CSP with 20 wt.% of water as a transient liquid.

Mechanical Pressure (MPa)	Temperature (°C)	Average Crystallite Size (nm) γ-AlOOH	Average Crystallite Size (nm) α-Al_2O_3	Density (g cm^{-1})	Relative Density (%)	Open Porosity (%)
90	450	-	-	2.23	58.2	41.0
220	380	-	4.20	2.53	63.7	36.0
	410	6.48	5.68	2.51	64.0	35.7
	450	-	6.68	2.58	65.0	34.6
350	380	4.17	6.08	1.95	62.6	35.3
	410	4.94	7.17	1.98	63.6	28.4
	450	3.66	5.49	2.08	64.4	22.8

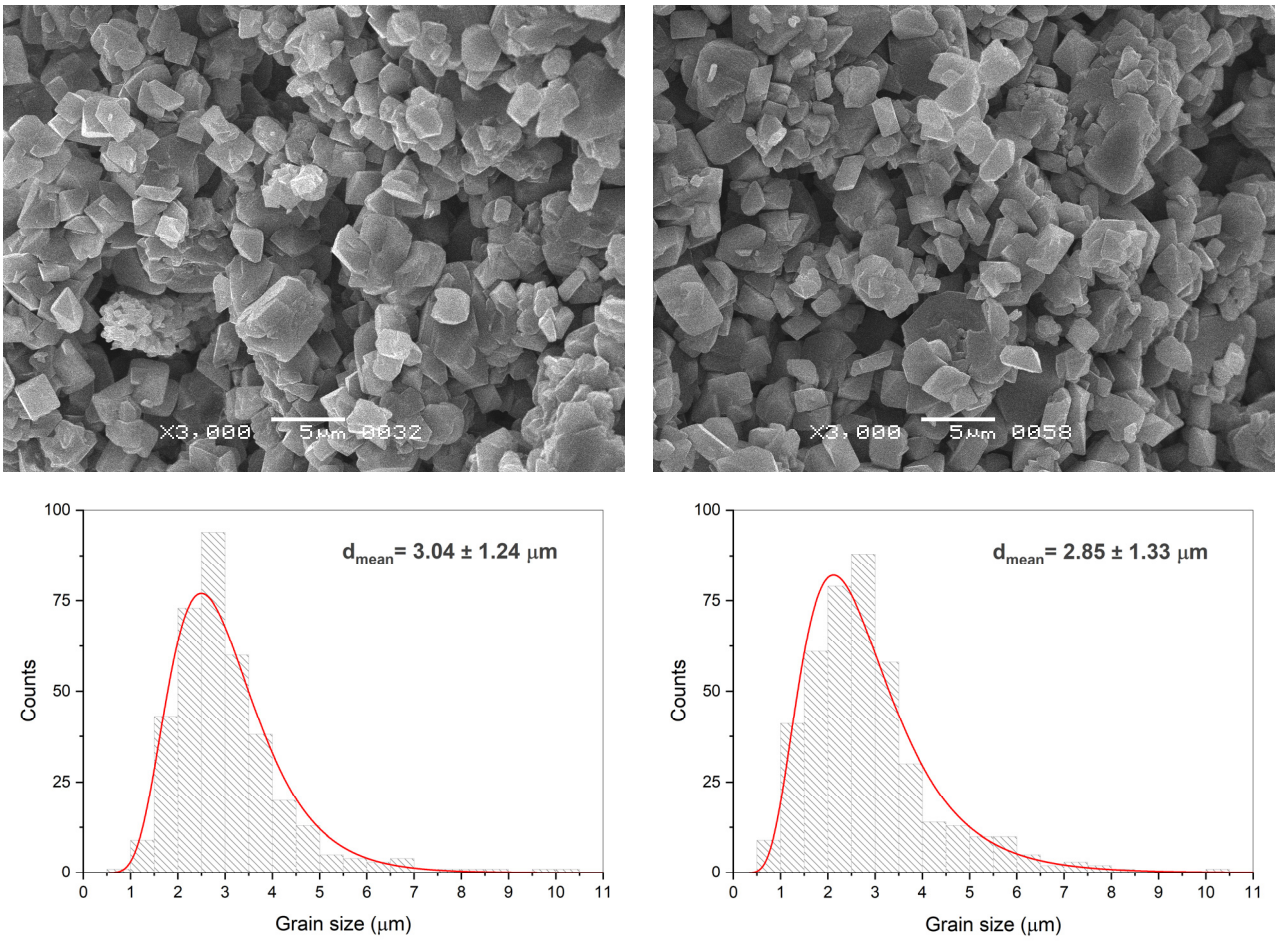
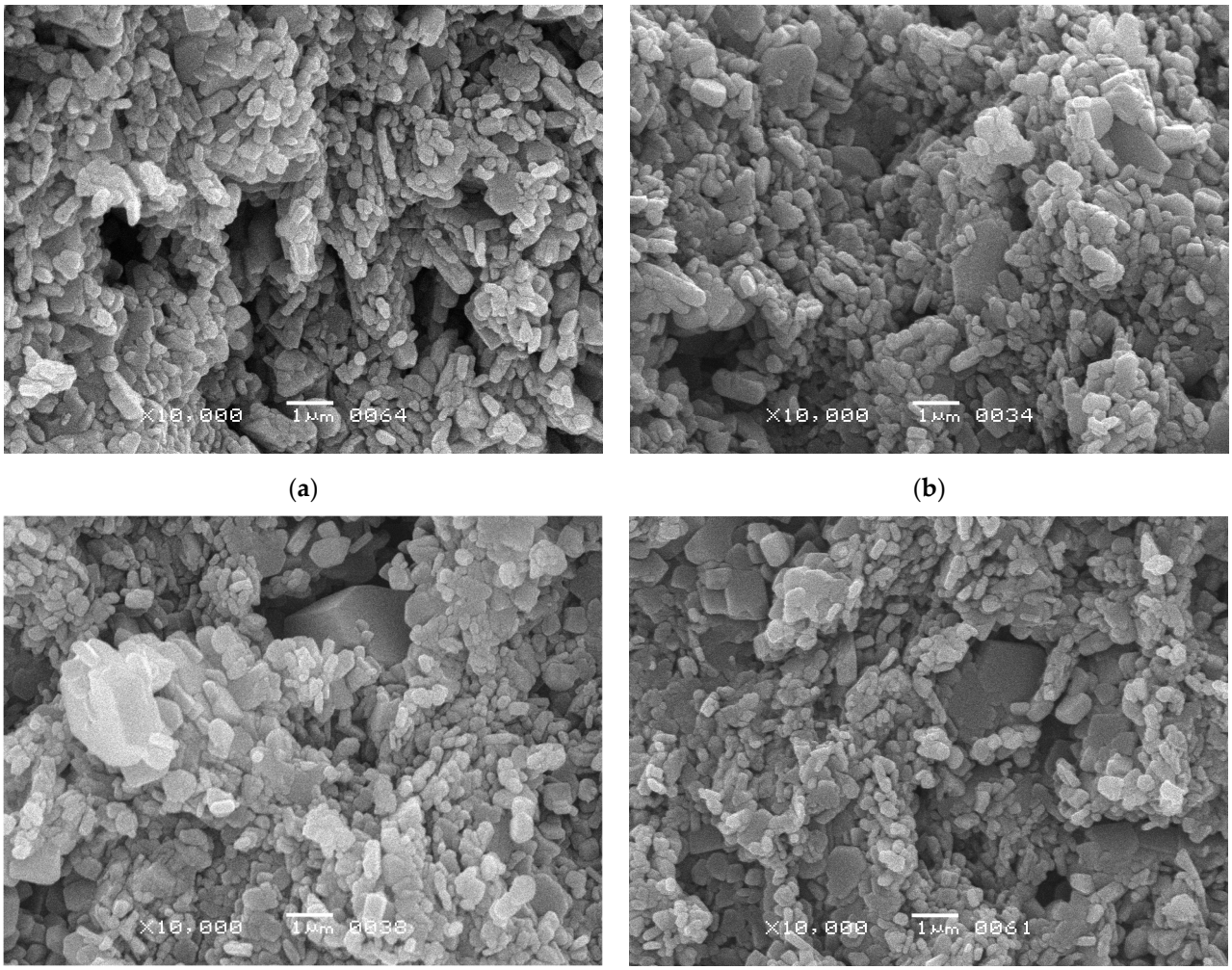


Figure 5. Fractured surfaces SEM images of the ceramics manufactured by CSP at a mechanical pressure of 220 MPa and a temperature of 380 °C (**a**) and 450 °C (**b**). Corresponding grain size distributions were calculated on the basis of 400 measurements of the grain size in each of the samples.

Formed at 350 MPa and 380 °C, the boehmite ceramics consist of submicron-sized grains with a smoothed slightly elongated shape (Figure 6a). Fine-grained regions are separated by a large pore space. Neighboring grains support a unidirectional orientation. An increase in the CSP temperature to 410 °C led to the appearance of single plate-like grains

of 2–4 μm in diameter among the fine matrix (Figure 6b). After CSP at 450 °C, the trend to the mutual orientation of neighboring grains continues among submicron rounded as well as micron-sized plate-like ones leading to their coalescence and the formation of faceted grains (Figure 6c,d). The latter are attributed to α-Al_2O_3 whose phase fraction significantly increased after the CSP at 450 °C compared to processing at lower temperatures. The size of the mentioned alumina grains was comparable to that determined for α-Al_2O_3 formed at 220 MPa (Figure 5).



(**a**) (**b**)

(**c**) (**d**)

Figure 6. SEM images of fractured surfaces of ceramics manufactured by CSP at a mechanical pressure of 350 MPa and a temperature of 380 °C (**a**), 410 °C (**b**), and 450 °C (**c**,**d**).

4. Discussion

Being heated in air at about 300 °C, gibbsite γ-$Al(OH)_3$ is commonly known to decompose into boehmite γ-AlOOH. Boehmite eliminates water at about 500–550 °C with the formation of γ-Al_2O_3. The latter undergoes a sequence of transformations to δ- and θ-alumina modifications and finally forms α-Al_2O_3 above 1050 °C [41,42]. In this way, transitional phases perform the face-centered cubic packing of oxygen ions. Another way from γ-$Al(OH)_3$ to α-Al_2O_3 in an air atmosphere includes the formation of χ- and κ-alumina phases with hexagonal close-packed oxygen ions above 300 °C [41]. In a water medium (below and above the critical point of 374 °C, 22.1 MPa), the route from gibbsite to α-Al_2O_3 was reported to pass only through the formation of boehmite, which transforms directly into α-alumina [34,43,44]. In the current work, the heating of γ-$Al(OH)_3$ powder occurred in the presence of supercritical water as the applied mechanical pressure (>90 MPa) and

the temperature of isothermal dwell (>380 °C) exceeded critical parameters. Under these conditions, the formation of three phases was observed, i.e., γ-AlOOH, χ-, and α-Al_2O_3. All these phases were detected in the ceramics processed at 450 °C and 90 MPa. It is worth noting that the starting gibbsite experienced heating with a relatively high rate. Earlier, Ingram-Jones et al. [45] reported that the fast heating of fine γ-$Al(OH)_3$ (0.5 μm) powder first resulted in its transformation to χ-Al_2O_3. Coarse gibbsite particles (14 μm) are prone to form boehmite as well as χ-Al_2O_3 at the initial step of their thermal decomposition. The gibbsite powder used in the current work consisted of particles with an average size of 1.93 μm (Figure A1). Thus, the formation of χ-Al_2O_3 during its relatively fast heating appears expectable. Along with χ-Al_2O_3, γ-AlOOH is supposed to form from gibbsite at 90 MPa and then completely decompose into α-Al_2O_3. In the samples prepared at a higher mechanical pressure, χ-Al_2O_3 was not found. At 220 MPa and 450 °C, a single-phase α-Al_2O_3 formed from an intermediate boehmite phase. However, after CSP at 350 MPa and 450 °C, α-Al_2O_3 became a minor phase in the ceramic sample. The mentioned observations indicated that the initial step in the CSP of gibbsite was its dehydroxylation. The route of γ-$Al(OH)_3$ decomposition depended on the mechanical pressure. The rise in the applied pressure hindered the elimination of OH-groups from the solid because of the related increase in the supercritical water density inside of the mold. Regardless of temperature, α-Al_2O_3 was the main phase in the ceramics obtained at 220 MPa. The ceramic samples prepared at 350 MPa contained boehmite as the major phase. Similarly, dehydroxylation processes in γ-AlOOH as well as in $BaTiO_3$ exposed to supercritical water were reported to depend on the density of the medium [46].

The phase transformation of boehmite into α-alumina in a water medium under supercritical conditions has been extensively studied previously [34,44,47]. The observed evolution of the powders' morphology derived two separate viewpoints on alumina formation and growth. On one hand, Suchanek [44] found no evident orientation of boehmite particles on surfaces of α-alumina crystals to prove the solid-state nature of alumina nucleation and growth. In the mentioned work, dissolution–precipitation or surface diffusion processes were supposed to govern the reaction. Plyasunov [48] reported that the dissolved form of α-alumina in the supercritical water is $Al(OH)_3 \cdot H_2O$. On another hand, Ivakin et al. [34] revealed the homogenous nucleation of α-Al_2O_3 in boehmite particles. The currently obtained ceramic samples contained phases different from $Al(OH)_3$. The presence of $Al(OH)_3$ might point to the dissolution–precipitation mechanism in this case. However, the microstructure observed in the samples obtained at 380 °C and 350 MPa (Figure 6a) resembled that demonstrated by Yamaguchi et al. [9] for the porous boehmite material CSPed from γ-$Al(OH)_3$ at milder conditions (250 °C, 270 MPa). The authors assumed that the large pores in the material were relics of the completely dissolved gibbsite particles. Boehmite grains nucleate and grow from the solution separating the gibbsite particles. It is important to note that the pore space in boehmite-based material could result from an intensive elimination of water during gibbsite decomposition.

A study of the microstructural changes during CSP at different temperatures and pressure values shows that the dehydroxylation of the initial gibbsite on heating first results in the development of a fine-grained boehmite structure (Figure 7a). Further processing leads to the coalescence of these submicron grains and the formation of larger plate-like grains of boehmite (Figure 7b). From [14,32], this stage of CSP is accompanied by an interaction of the solid with the water molecules from the medium. This process includes a dissociative adsorption of H_2O as well as the condensation of H^+ and OH^- with the formation of bridging oxygen between the metal ions. As a result, the mentioned processes have a decisive role in oxygen ions' diffusion, which facilitates the mass transport between the grains and lowers the activation energy of phase transitions. Boehmite grains of both rounded and plate-like morphologies tend to perform coalescence and finally transform homogenously into an α-alumina modification under the CSP conditions (Figure 7c). Earlier, the coalescence of particles was also demonstrated for the CSP of ZnO [49], $CaCO_3$ [6], and $Na_2Mo_2O_7$ [50].

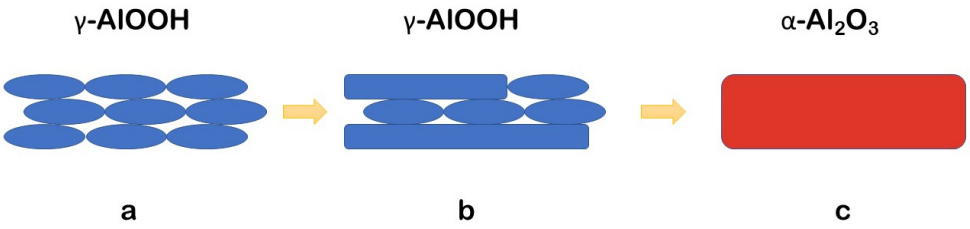


Figure 7. A schematic representation of the microstructural transformations during the CSP: (**a**) formation of fine-grained boehmite structure; (**b**) formation of plate-like boehmite grains by coalescence; (**c**) α-Al_2O_3 formation.

Regardless of the phase composition, the obtained ceramics possessed a relative density in the range of 58–65%. These density values are close to the density of conventionally pressed compacts. It is likely that the porosity of samples containing boehmite was supported by water elimination accompanying ongoing transformation into α-alumina. The shape of the formed α-Al_2O_3 grains resembled α-Al_2O_3 crystals synthesized from boehmite powder in a medium of supercritical water [34,44]. Compared to the parent boehmite grains, the grains of α-alumina increased in size and approached their Wulffs shape [51]. The Wulffs shape indicates the fall of the driving force for the sintering and corresponds to the remaining porosity.

The α-Al_2O_3 ceramics currently produced by CSP demonstrated a porosity which is almost totally of the open type and is comparable to the recent results obtained by a traditional route [24,52–54]. This would make the obtained material highly attractive as a filter, thermal insulator, a component of polymer- and metal-ceramic composite, etc. The energy- and time-saving CSP technique would also be a reason for the competitiveness of these alumina ceramics compared to the related alumina materials conventionally sintered at a high temperature.

5. Conclusions

(1) For the first time, porous α-Al_2O_3 ceramics were processed directly by CSP at a temperature of 380–450 °C and a pressure of 220 MPa during 30 min in the presence of pure water. The materials were characterized by predominately open-type porosity reaching 36%.

(2) Under the studied CSP conditions, the initial γ-$Al(OH)_3$ powder undergoes dehydration leading to γ-AlOOH and possible minor χ-Al_2O_3 phases. Further processed, γ-AlOOH forms elongated grains, which coalesce into plate-like ones and transform into grains of α-Al_2O_3.

(3) An increase in the applied pressure (up to 350 MPa) prevents the dehydration of γ-AlOOH and impedes the formation of the final α-Al_2O_3.

Author Contributions: Conceptualization, A.V.S. and Y.D.I.; methodology, A.A.K., M.V.K. and Y.D.I.; validation, M.V.K.; formal analysis, A.N.K. and L.A.A.; investigation, A.A.K., M.V.K., A.N.K., L.A.A. and Y.D.I.; resources, A.A.K., M.V.K. and Y.D.I.; data curation, A.A.K., M.V.K., A.N.K., L.A.A. and Y.D.I.; writing—original draft preparation, A.A.K.; writing—review and editing, A.A.K., A.V.S. and Y.D.I.; visualization, A.A.K.; supervision, A.V.S. and Y.D.I.; project administration, A.A.K.; funding acquisition, A.A.K. All authors have read and agreed to the published version of the manuscript.

Funding: This research was funded by the Russian Science Foundation, Grant Number 22-73-00318.

Institutional Review Board Statement: Not applicable.

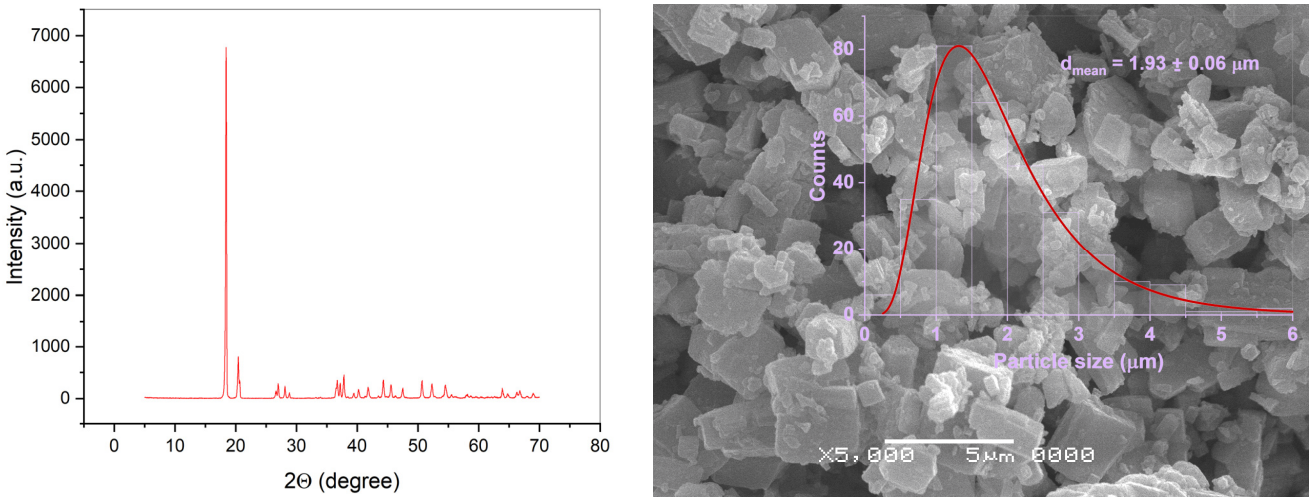
Informed Consent Statement: Not applicable.

Data Availability Statement: The data presented in this study are available in this article.

Acknowledgments: The authors would like to thank Tatiana V. Filippova from the Chemistry Department of Lomonosov MSU for her kind help with XRD analysis. The study was supported in part by Lomonosov Moscow State University Program of Development.

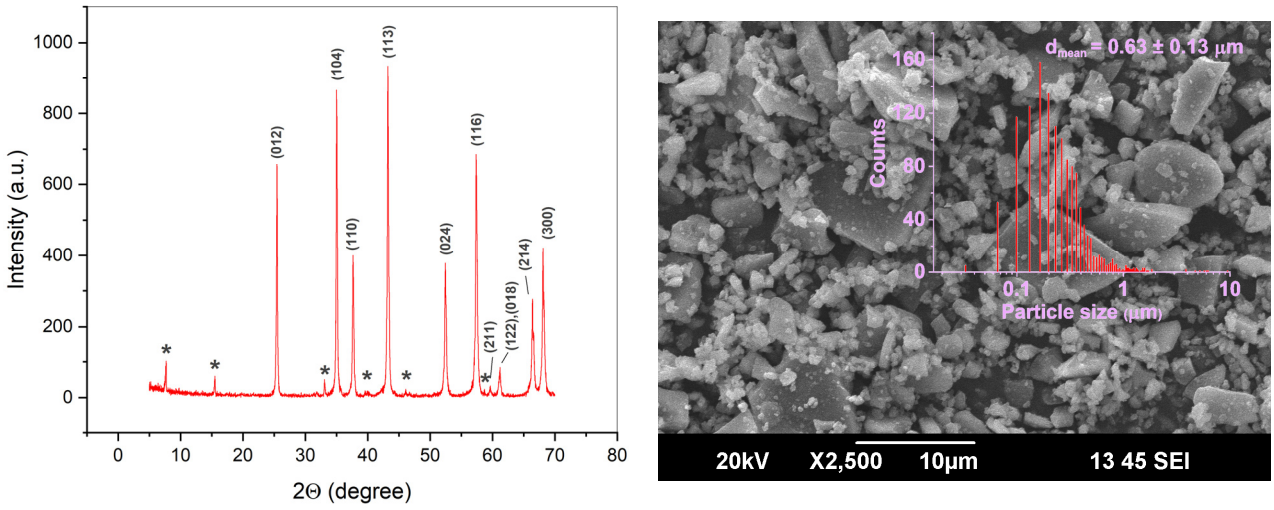
Conflicts of Interest: The authors declare no conflicts of interest.

Appendix A



(**a**) (**b**)

Figure A1. XRD pattern (**a**) and SEM image (**b**) of the initial gibbsite (γ-$Al(OH)_3$) powder. The observed peaks correspond to PDF2 #000-076-1782. The size distribution is based on the measurements of 300 particles.



(**a**) (**b**)

Figure A2. XRD pattern (**a**) and SEM image (**b**) of a commercial α-Al_2O_3 additive with the initial γ-$Al(OH)_3$ powder. Miller indices correspond to the α-Al_2O_3 phase (PDF2 #000-075-0782), asterisks indicate the $Al_{22}O_{34}(H_2O)_2$ phase (PDF2 #000-070-1204). The calculated major phase content is 90.5 wt.%. The size distribution is based on the measurements of 1300 particles.

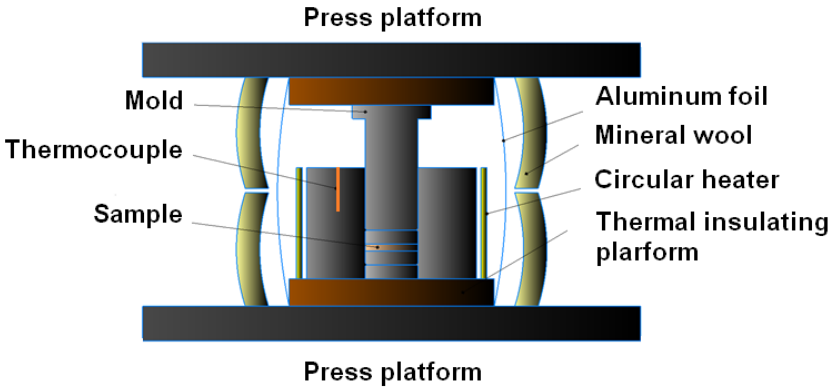


Figure A3. Schematic representation of the mold prepared for CSP.

References

1. Randall, C.A.; Guo, J.; Baker, A.; Lanagan, M.T.; Guo, H. Cold Sintering Ceramics and Composites. U.S. Patent 2017/0088471A1, 30 March 2017.
2. Huang, Y.; Huang, K.; Zhou, S.; Lin, C.; Wu, X.; Gao, M.; Zhao, C.; Fang, C. Influence of Incongruent Dissolution-Precipitation on 8YSZ Ceramics during Cold Sintering Process. *J. Eur. Ceram. Soc.* **2022**, *42*, 2362–2369. [CrossRef]
3. Nie, B.; Liu, T.; Alcoutlabi, M.; Basu, S.; Kumara, S.; Li, M.; Lian, J.; Sun, H. Cold Sintering-Enabled Interface Engineering of Composites for Solid-State Batteries. *Front. Energy Res.* **2023**, *11*, 1149103. [CrossRef]
4. Grasso, S.; Biesuz, M.; Zoli, L.; Taveri, G.; Duff, A.I.; Ke, D.; Jiang, A.; Reece, M.J. A Review of Cold Sintering Processes. *Adv. Appl. Ceram.* **2020**, *119*, 115–143. [CrossRef]
5. Galotta, A.; Sglavo, V.M. The Cold Sintering Process: A Review on Processing Features, Densification Mechanisms and Perspectives. *J. Eur. Ceram. Soc.* **2021**, *41*, 1–17. [CrossRef]
6. Zahabi, M.; Said, A.; Memari, A. Cold Sintering of Calcium Carbonate for Construction Material Applications. *ACS Omega* **2021**, *6*, 2576–2588. [CrossRef] [PubMed]
7. Yamaguchi, K.; Hashimoto, S. Mechanism of Densification of Calcium Carbonate by Cold Sintering Process. *J. Eur. Ceram. Soc.* **2022**, *42*, 6048–6055. [CrossRef]
8. Smirnov, A.V.; Ivakin, Y.D.; Kornyushin, M.V.; Kholodkova, A.A.; Vasin, A.A.; Ayudinyan, S.; Kirakosyan, H.V. Effect of Activating Additives on the Cold Sintering Process of $(MnFeCoNiCu)_3O_4$ High-Entropy Ceramics. *Fine Chem. Technol.* **2022**, *17*, 439–449. [CrossRef]
9. Yamaguchi, K.; Hashimoto, S. Effect of Phase Transformation in Cold Sintering of Aluminum Hydroxide. *J. Eur. Ceram. Soc.* **2024**, *44*, 2754–2761. [CrossRef]
10. Thabet, K.; Quarez, E.; Joubert, O.; Le Gal La Salle, A. Application of the Cold Sintering Process to the Electrolyte Material $BaCe_{0.8}Zr_{0.1}Y_{0.1}O_{3-\delta}$. *J. Eur. Ceram. Soc.* **2020**, *40*, 3445–3452. [CrossRef]
11. Guo, H.; Bayer, T.J.M.; Guo, J.; Baker, A.; Randall, C.A. Cold Sintering Process for 8 mol%Y_2O_3-Stabilized ZrO_2 Ceramics. *J. Eur. Ceram. Soc.* **2017**, *37*, 2303–2308. [CrossRef]
12. Lai, Q.; Chen, J.; Chang, F.; Pei, J.; Liang, Y.; Chen, X.; Feng, Q.; Cen, Z.; Luo, N. Cold Sintering Process Assisted Sintering for 8YSZ Ceramic: A Way of Achieving High Density and Electrical Conductivity at a Reduced Sintering Temperature. *Ceram. Int.* **2023**, *49*, 14744–14749. [CrossRef]
13. Grady, Z.; Ndayishimiye, A.; Randall, C. A Dramatic Reduction in the Sintering Temperature of the Refractory Sodium B″-Alumina Solid Electrolyte via Cold Sintering. *J. Mater. Chem. A* **2021**, *9*, 22002–22014. [CrossRef]
14. Guo, N.; Liu, M.; Shen, J.-Y.; Shen, H.-Z.; Shen, P. Surface Hydrate-Assisted Low- and Medium-Temperature Sintering of MgO. *Scr. Mater.* **2022**, *206*, 114258. [CrossRef]
15. Amrute, A.P.; Jeske, K.; Łodziana, Z.; Prieto, G.; Schüth, F. Hydrothermal Stability of High-Surface-Area α-Al_2O_3 and Its Use as a Support for Hydrothermally Stable Fischer–Tropsch Synthesis Catalysts. *Chem. Mater.* **2020**, *32*, 4369–4374. [CrossRef]
16. Huang, C.-L.; Wang, J.-J.; Huang, C.-Y. Sintering Behavior and Microwave Dielectric Properties of Nano Alpha-Alumina. *Mater. Lett.* **2005**, *59*, 3746–3749. [CrossRef]
17. Asimakopoulou, A.; Gkekas, I.; Kastrinaki, G.; Prigione, A.; Zaspalis, V.T.; Petrakis, S. Biocompatibility of α-Al_2O_3 Ceramic Substrates with Human Neural Precursor Cells. *J. Funct. Biomater.* **2020**, *11*, 65. [CrossRef]
18. Hashimoto, H.; Kojima, S.; Sasaki, T.; Asoh, H. α-Alumina Membrane Having a Hierarchical Structure of Straight Macropores and Mesopores inside the Pore Wall. *J. Eur. Ceram. Soc.* **2018**, *38*, 1836–1840. [CrossRef]
19. Rytter, E.; Borg, Ø.; Enger, B.C.; Holmen, A. α-Alumina as Catalyst Support in Co Fischer-Tropsch Synthesis and the Effect of Added Water; Encompassing Transient Effects. *J. Catal.* **2019**, *373*, 13–24. [CrossRef]
20. Liu, Y.; Ng, Z.; Khan, E.A.; Jeong, H.-K.; Ching, C.; Lai, Z. Synthesis of Continuous MOF-5 Membranes on Porous α-Alumina Substrates. *Microporous Mesoporous Mater.* **2009**, *118*, 296–301. [CrossRef]

21. Dong, J.; Payzant, E.A.; Hu, M.Z.C.; Depaoli, D.W.; Lin, Y.S. Synthesis of MFI-Type Zeolite Membranes on Porous α-Alumina Supports by Wet Gel Crystallization in the Vapor Phase. *J. Mater. Sci.* **2003**, *38*, 979–985. [CrossRef]
22. Ohji, T.; Fukushima, M. Macro-Porous Ceramics: Processing and Properties. *Int. Mater. Rev.* **2012**, *57*, 115–131. [CrossRef]
23. Niu, L.; Qin, R.; Liu, Y.; Xin, J.; Wu, X.; Zhang, F.; Li, X.; Shao, C.; Li, X.; Liu, Y. Hierarchical Porous Alumina Ceramics as Multi-Functional Support with Excellent Performance. *Ceram. Int.* **2024**, *50*, 2611–2622. [CrossRef]
24. Zhao, J.; Wang, L.; Mao, X.; An, L.; Liu, Y.; Wang, S.; Zhang, J.; Feng, K. Preparation and Properties of Porous Alumina Ceramics for Ultra-Precision Aerostatic Bearings. *Ceram. Int.* **2022**, *48*, 13311–13318. [CrossRef]
25. Zhang, A.; Sang, K.; Zeng, D.; Liu, Q.; Guo, Y. Preparation and Properties of Porous Alumina with Inter-Locked Platelets Structure. *Ceram. Int.* **2022**, *48*, 25918–25922. [CrossRef]
26. Dong, X.; Chua, B.W.; Li, T.; Zhai, W. Multi-Directional Freeze Casting of Porous Ceramics with Bone-Inspired Microstructure. *Mater. Des.* **2022**, *224*, 111344. [CrossRef]
27. Chen, H.; Pan, Y.; Chen, B.; Li, J.; Gui, Z.; Chen, J.; Yan, H.; Zeng, Y.; Chen, J. Fabrication of Porous Aluminum Ceramics beyond Device Resolution via Stereolithography 3D Printing. *Ceram. Int.* **2023**, *49*, 18463–18469. [CrossRef]
28. Moshkovitz, M.Y.; Paz, D.; Magdassi, S. 3D Printing Transparent γ-Alumina Porous Structures Based on Photopolymerizable Sol–Gel Inks. *Adv. Mater. Technol.* **2023**, *8*, 2300123. [CrossRef]
29. Hérisson de Beauvoir, T.; Estournès, C. Translucent γ-AlOOH and γ-Al_2O_3 Glass-Ceramics Using the Cold Sintering Process. *Scr. Mater.* **2021**, *194*, 113650. [CrossRef]
30. Kang, S.; Zhao, X.; Guo, J.; Liang, J.; Sun, J.; Yang, Y.; Yang, L.; Liao, R.; Randall, C.A. Thermal-Assisted Cold Sintering Study of Al_2O_3 Ceramics: Enabled with a Soluble γ-Al_2O_3 Intermediate Phase. *J. Eur. Ceram. Soc.* **2023**, *43*, 478–485. [CrossRef]
31. Suleiman, B.; Zhang, H.; Ding, Y.; Li, Y. Microstructure and Mechanical Properties of Cold Sintered Porous Alumina Ceramics. *Ceram. Int.* **2022**, *48*, 13531–13540. [CrossRef]
32. Gao, J.; Ding, Q.; Yan, P.; Liu, Y.; Hu, Y.; Ren, Y.; Wang, X.; Mustafa, T.; Fan, Y.; Jiang, W. Direct Cold Sintering of Translucent Gamma-Al_2O_3 Ceramics. *J. Eur. Ceram. Soc.* **2024**, *44*, 4225–4231. [CrossRef]
33. Kholodkova, A.A.; Kornyushin, M.V.; Pakhomov, M.A.; Smirnov, A.V.; Ivakin, Y.D. Water-Assisted Cold Sintering of Alumina Ceramics in SPS Conditions. *Ceramics* **2023**, *6*, 1113–1128. [CrossRef]
34. Ivakin, Y.D.; Danchevskaya, M.N.; Muravieva, G.P. Induced Formation of Corundum Crystals in Supercritical Water Fluid. *Russ. J. Phys. Chem. B* **2015**, *9*, 1082–1094. [CrossRef]
35. Yoshizawa, Y.; Hirao, K.; Kanzaki, S. Fabrication of Low Cost Fine-Grained Alumina Powders by Seeding for High Performance Sintered Bodies. *J. Eur. Ceram. Soc.* **2004**, *24*, 325–330. [CrossRef]
36. Gates-Rector, S.; Blanton, T. The Powder Diffraction File: A Quality Materials Characterization Database. *Powder Diffr.* **2019**, *34*, 352–360. [CrossRef]
37. Rodríguez-Carvajal, J. Recent Advances in Magnetic Structure Determination by Neutron Powder Diffraction. *Phys. B Condens. Matter* **1993**, *192*, 55–69. [CrossRef]
38. Vaitkus, A.; Merkys, A.; Sander, T.; Quirós, M.; Thiessen, P.A.; Bolton, E.E.; Gražulis, S. A Workflow for Deriving Chemical Entities from Crystallographic Data and Its Application to the Crystallography Open Database. *J. Cheminform.* **2023**, *15*, 123. [CrossRef]
39. Rietveld, H.M. A Profile Refinement Method for Nuclear and Magnetic Structures. *J. Appl. Crystallogr.* **1969**, *2*, 65–71. [CrossRef]
40. Schneider, C.A.; Rasband, W.S.; Eliceiri, K.W. NIH Image to ImageJ: 25 Years of Image Analysis. *Nat. Methods* **2012**, *9*, 671–675. [CrossRef]
41. MacKenzie, K.J.D.; Temuujin, J.; Okada, K. Thermal Decomposition of Mechanically Activated Gibbsite. *Thermochim. Acta* **1999**, *327*, 103–108. [CrossRef]
42. Lamouri, S.; Hamidouche, M.; Bouaouadja, N.; Belhouchet, H.; Garnier, V.; Fantozzi, G.; Trelkat, J.F. Control of the γ-Alumina to α-Alumina Phase Transformation for an Optimized Alumina Densification. *Boletín de la Sociedad Española de Cerámica y Vidrio* **2017**, *56*, 47–54. [CrossRef]
43. Chen, B.; Xu, X.; Chen, X.; Kong, L.; Chen, D. Transformation Behavior of Gibbsite to Boehmite by Steam-Assisted Synthesis. *J. Solid State Chem.* **2018**, *265*, 237–243. [CrossRef]
44. Suchanek, W.L. Hydrothermal Synthesis of Alpha Alumina (α-Al_2O_3) Powders: Study of the Processing Variables and Growth Mechanisms. *J. Am. Ceram. Soc.* **2010**, *93*, 399–412. [CrossRef]
45. Ingram-Jones, V.J.; Slade, R.C.T.; Davies, T.W.; Southern, J.C.; Salvador, S. Dehydroxylation Sequences of Gibbsite and Boehmite: Study of Differences between Soak and Flash Calcination and of Particle-Size Effects. *J. Mater. Chem.* **1996**, *6*, 73. [CrossRef]
46. Hayashi, H.; Hakuta, Y. Hydrothermal Synthesis of Metal Oxide Nanoparticles in Supercritical Water. *Materials* **2010**, *3*, 3794–3817. [CrossRef] [PubMed]
47. Ivakin, Y.D.; Danchevskaya, M.N.; Muravieva, G.P. Recrystallization of Zinc Oxide in a Sub- and Supercritical Water Medium. *Russ. J. Phys. Chem. B* **2019**, *13*, 1189–1200. [CrossRef]
48. Plyasunov, A.V. Predicting Solubility of Oxides of Metals and Metalloids in Supercritical Water. *Ind. Eng. Chem. Res.* **2020**, *59*, 970–980. [CrossRef]
49. Smirnov, A.V.; Kornyushin, M.V.; Kholodkova, A.A.; Melnikov, S.A.; Stepanov, A.D.; Fesik, E.V.; Ivakin, Y.D. Cold Sintering Process of Zinc Oxide Ceramics: Powder Preparation and Sintering Conditions Effects on Final Microstructure. *Inorganics* **2022**, *10*, 197. [CrossRef]

50. Ndayishimiye, A.; Fan, Z.; Mena-Garcia, J.; Anderson, J.M.; Randall, C.A. Coalescence in Cold Sintering: A Study on Sodium Molybdate. *Open Ceram.* **2022**, *11*, 100293. [CrossRef]
51. Marmier, A.; Parker, S.C. Ab Initio Morphology and Surface Thermodynamics of $\alpha - Al_2O_3$. *Phys. Rev. B* **2004**, *69*, 115409. [CrossRef]
52. Alzukaimi, J.; Jabrah, R. The Preparation and Characterization of Porous Alumina Ceramics Using an Eco-friendly Pore-forming Agent. *Int. J. Appl. Ceram. Technol.* **2019**, *16*, 820–831. [CrossRef]
53. Kerolli Mustafa, M.; Gabelica, I.; Mandić, V.; Veseli, R.; Ćurković, L. Reusing Waste Coffee Grounds in the Preparation of Porous Alumina Ceramics. *Sustainability* **2022**, *14*, 14244. [CrossRef]
54. Vemoori, R.; Bejugama, S.; Khanra, A.K. Fabrication and Characterization of Alumina and Zirconia-Toughened Alumina Porous Structures. *Ceram. Int.* **2023**, *49*, 21708–21715. [CrossRef]

Disclaimer/Publisher's Note: The statements, opinions and data contained in all publications are solely those of the individual author(s) and contributor(s) and not of MDPI and/or the editor(s). MDPI and/or the editor(s) disclaim responsibility for any injury to people or property resulting from any ideas, methods, instructions or products referred to in the content.